Requirements for discrete actuator and segmented wavefront correctors for aberration compensation in two large populations of human eyes

Nathan Doble[1,2,*], **Donald T. Miller**[3], **Geunyoung Yoon**[4], and **David R. Williams**[1]

[1]*Center for Visual Science, 274 Meliora Hall, University of Rochester, Rochester, New York 14627, USA*

[3]*School of Optometry, Indiana University, Bloomington, Indiana 47405, USA*

[4]*Department of Ophthalmology, University of Rochester, Rochester, New York 14642, USA*

Abstract

Numerous types of wavefront correctors have been employed in adaptive optics (AO) systems for correcting the ocular wavefront aberration. While all have improved image quality, none have yielded diffraction-limited imaging for large pupils (≥6 mm), where the aberrations are most severe and the benefit of AO the greatest. To this end, we modeled the performance of discrete actuator, segmented piston-only, and segmented piston/tip/tilt wavefront correctors in conjunction with wavefront aberrations measured on normal human eyes in two large populations. The wavefront error was found to be as large as 53 μm, depending heavily on the pupil diameter (2–7.5 mm) and the particular refractive state. The required actuator number for diffraction-limited imaging was determined for three pupil sizes (4.5, 6, and 7.5 mm), three second-order aberration states, and four imaging wavelengths (0.4, 0.6, 0.8, and 1.0 μm). The number across the pupil varied from only a few actuators in the discrete case to greater than 100 for the piston-only corrector. The results presented will help guide the development of wavefront correctors for the next generation of ophthalmic instrumentation.

1. Introduction

The optical resolution of the eye is fundamentally limited by the wave aberrations intrinsic to the cornea and crystalline lens and diffraction due to the finite size of the eye's pupil. Conventional corrective methods such as spectacles, contact lenses, and refractive surgery provide a static amelioration of low-order sphere and cylinder. However, ocular image quality can be significantly improved by dilating the pupil to minimize diffraction and correcting the aberrations across the larger pupil, for example, using an adaptive optics (AO) system [1].

AO has been successfully integrated into a variety of retina camera modalities, including conventional fundus cameras [1-7], confocal scanning laser ophthalmoscopes (cSLO) [8-10], and optical coherence tomography (OCT) [11-17]. The technique enables routine, *in vivo* observation of retinal structure at the cellular level, structure that could not otherwise be seen. AO has also been used to explore the limits of human visual acuity [18] and to control the type and amount of aberrations to which the retina is exposed [19,20]. For design considerations and a review of results using AO in vision science the reader is directed to Refs. 21 and 22.

*Corresponding author: nathan.doble@irisao.com.
[2]Current address: Iris AO, Inc., 2680 Bancroft Way, Berkeley, California 94704, USA

The effectiveness of AO fundamentally depends on its ability to measure, track, and correct the ocular aberrations. Performance of the last step is largely dictated by the AO system's key component, its wavefront corrector. This device dynamically imparts an ideally conjugate aberration profile onto the passing wavefront, thus canceling the original aberrations. Numerous types of wavefront correctors have been employed in AO systems for the eye, but none have yielded diffraction-limited imaging for large pupils (≥6 mm). One problem is that the characteristics of the wavefront corrector necessary to achieve diffraction-limited imaging in the human eye are not well understood. Consequently, correctors have been employed somewhat arbitrarily with the expectation that image quality will improve, the extent of which is empirically determined.

Additionally, many of the wavefront correctors applied to the eye have been developed primarily for compensation of atmospheric turbulence. A common example being macroscopic discrete actuator deformable mirrors (DMs), such as those manufactured by Xinetics Inc. [23]. Specifically, their actuator number, stroke, influence functions, and speed have been tailored to the spatial and temporal properties of the atmosphere [24,25] rather than that of the eye [26,27]. The high temporal fluctuations of atmospheric turbulence are roughly 2 orders greater than the microfluctuations in the eye; also their dynamic range is often too small for compensation of ocular aberrations. While wavefront correctors represent a small fraction of the total cost of ground-based telescopes in which they are employed, they represent a significant fraction of the total cost of most commercial retina cameras. Atmospheric wavefront correctors are also generally bulky, with large mirror surfaces (approximately several centimeters or more) that require long focal length relay optics to magnify the pupil of the eye. A smaller corrector comparable with the dilated pupil of the eye (4–8 mm) can substantially reduce the instrument size and is commercially attractive.

Alternative wavefront corrector technologies, which are more cost effective and smaller, have been explored. Burns *et al.* [28] evaluated a customized phase plate to correct static higher-order aberrations for a cSLO. Significant improvement, however, can be realized if the correction is performed dynamically [2]. Various types of dynamic wavefront correctors have hence been applied to the eye. Bimorph mirrors [24,25] having 13–35 actuators have been investigated by several groups [3-5,14,15]. Recently, Fernandez *et al.* [29] evaluated a magnetic membrane mirror with 52 actuators. Microelectromechanical systems (MEMS) [30], promises batch fabrication of low cost, compact wavefront correctors. Bulk micromachined membrane MEMS mirrors [31] employing 37 electrodes have been successfully applied to the eye [32-34]. Although both bimorph and membrane mirrors have a large dynamic range (~8 and 16 μm, respectively [32,35]) for low-order aberrations, this falls rapidly with increasing spatial frequency. For an analysis of several commercial bimorph and bulk micromachined MEMS mirrors for the eye, see Dalimier and Dainty [35].

Surface micromachined devices [30] are another class of MEMS mirror whose mode of operation is comparable with discrete actuator DMs. Doble *et al.* [36] employed a surface micromachined MEMS DM [37] and successfully imaged human cone photoreceptors, demonstrating that wavefront correctors other than the macroscopic form are capable of this task.

Liquid-crystal spatial light modulators (LC-SLMs) are an alternative wavefront corrector technology. Transmissive, pixelated designs with 69 and 127 pixels were examined by Thibos and Bradley [38] and Vargas *et al.* [39], respectively. Prieto *et al.* [40] and Fernández *et al.* [16] used an optically addressed LC-SLM [41]. Such devices have high spatial resolution (480 × 480 piston-only pixels) and low control voltages (~5 V) but are limited to phase-modulating polarized light with typical modulation confined to 2π. Phase wrapping [38,42] must be used to extend their dynamic range.

While most of these correctors hold considerable promise for vision science, it remains unclear what the optimal parameters are to achieve a specified performance level in the eye, e.g., diffraction-limited imaging. Miller *et al.* [42] provided a performance evaluation of piston-only segmented wavefront correctors using a limited population of 12 human eyes. Here we considerably extend this analysis to cover two separate large populations, each comprising 70 eyes. Two additional wavefront correctors, discrete actuator and piston/tip/tilt segmented devices are also examined. Required actuator stroke and number for diffraction-limited imaging is determined for various pupil sizes, second-order aberration states, and imaging wavelengths.

2. Methods

A. Description of the Two Populations

AO systems are used on a range of normal and pathologic eyes, and under different refractive conditions. As a first step to capture these differences in normal healthy eyes, our corrector analysis incorporated two large population studies.

The first study, based at the University of Rochester and Bausch & Lomb (unpublished), measured the 70 right eyes of normal subjects using the Bausch & Lomb Zywave aberrometer. The Zywave aberrometer uses a 600 μm pitch lenslet array (720 μm upon magnification) with a focal length of 40 mm. The CCD camera is a DMK 3002/C (The Imaging Source, Germany) with 752×582 pixels (8.6×8.3 μm, respectively). The beacon wavelength is 785 nm. The aberrometer returned all the aberration coefficients (including defocus and astigmatism) up to fifth order in the Zernike expansion for a 7.5 mm pupil diameter. The naming convention for the Zernike coefficients and polynomials recommended by the OSA/VSIA Standards Taskforce [43] was used. The overall wave aberration was measured without any form of refractive correction (e.g., trial lenses). Ages ranged from 20 to 59 years with a mean of 33.8 years and a standard deviation of 9.7 years. The dioptric range of spherical equivalent errors was −8.5 to −0.8 diopters (D) with a mean of −3.5 D and a standard deviation of 1.5 D. Similarly for a cylinder, the range was −2.75 to 0 D with a mean of −0.8 D and a standard deviation of 0.6 D. All subjects were myopic and candidates for laser refractive surgery. Subjects were dilated prior to measurement (2.5% phenylephrine and/or 1% tropicamide), and their heads stabilized with a chin and forehead rest. Five wavefront measurements were collected on each subject and averaged.

The second population study, described by Thibos *et al.* [44], involved 100 individuals drawn from the student body and faculty at the Indiana University School of Optometry. The Shack–Hartmann wavefront sensor in this study used a lenslet array with a 600 μm pitch (referenced to the plane of the eye's pupil) and a focal length of 24 mm. The wavefront sensor CCD camera was a MCD600 (Spectra-Source Instruments) with 1340×1037 pixels (6.8 μm $\times$ 6.8 μm pixels). All measurements were acquired at a wavelength of 633 nm. The mean age was 26.1 years with a standard deviation of 5.6 years. The range of spherical equivalent errors was −10 to +5.5 D with a mean of −3.1 D and a standard deviation of 3.0 D. The magnitude of cylinder ranged from 0 to 1.75 D with a mean of 0.3 D and a standard deviation of 0.38 D. From this population, 70 right eyes with pupil diameters of 7.5 mm were selected for our wavefront corrector analysis. Subjects were dilated and accommodation paralyzed by administration of cyclopentalate (0.5%, 1 drop). Aberrometry was performed with a laboratory Shack–Hartmann wavefront sensor in conjunction with trial lenses that were predetermined by a subjective refraction. A bite bar was used to stabilize the head. A minimum of three wavefront measurements were collected on each subject. Zernike modes up through tenth radial order were reconstructed by the method of least squares. Additional details can be found in Thibos *et al.* [44].

Figure 1 shows the wavefront variance decomposed by Zernike order for the Rochester and Indiana aberration studies. The magnitude of the wave aberrations for the Rochester population is noticeably larger than that for Indiana for all Zernike orders. While we do not know the source of this difference, it may stem from differences in the refraction protocol, age of the subjects, and possibly population type. A systematic bias between the two wavefront sensors is also possible (which was not investigated in this study), although both instruments were independently calibrated in previous studies. Another possibility is that the number of Zernike terms fitted to the Shack–Hartmann data is different for the two instruments. He *et al.* [45] have demonstrated systematic errors in the computations of low-order coefficients when a smaller set of Zernike coefficients is used, while there is finite power in the higher-order terms that are not extracted. While this scenario holds for the Rochester data in which only Zernike coefficients up through fifth order were computed, the power at higher orders (as present in the Indiana data) is appreciably small and certainly much smaller than the power difference observed between the Rochester and Indiana data at the low orders. It is unlikely therefore that this plays a contributing role.

When evaluating the three wavefront corrector types, three second-order aberrations states were considered: (i) all three second-order modes took their measured values, (ii) the defocus coefficient was set to zero, and (iii) all three second-order Zernike coefficients were set to zero. The motivation being that second-order aberrations almost always dominate the total wavefront error, yet their magnitude varies considerably depending on the refractive state of the subject and the manner in which trial lenses or translating lenses are applied. Collectively, these six scenarios (two populations, each with three second-order conditions) traverse a wide range of aberration strengths that are encountered in most imaging and vision experiments.

Note that both measured population data sets represent essentially static wave aberrations and therefore do not capture the temporal behavior of the ocular media. As such, the temporal responses of the wavefront correctors were not assessed in our modeling. This is not a fundamental limitation, however, as these devices (with the exception of LC-SLMs) have resonant frequencies well above the temporal dynamics of the eye's aberrations [26,27].

B. Wavefront Corrector Models

Figure 2 depicts the three types of wavefront correctors evaluated in this paper. The correctors are listed below, using a nomenclature similar to that by Hardy [24] and Tyson [25].

- Discrete actuator deformable mirrors have a continuous reflective surface whose profile is controlled by an underlying array of actuators (Fig. 2, top). Pushing one actuator produces a localized deflection of the mirror surface, termed the influence function. The deflection typically extends to adjacent actuators where it changes the mirror surface height by a fraction of the peak deflection. This fraction is termed the coupling coefficient.

- Piston-only, segmented correctors consist of an array of adjacent, planar mirror segments that are independently controlled (Fig. 2, middle). They have 1 degree of freedom that corresponds to pure, vertical piston. The influence function is a top hat with a zero coupling coefficient. The piston effect can also be realized with LC-SLMs that induce local optical path-length changes by altering the refractive index rather than translating mirror segments.

- Piston/tip/tilt, segmented correctors represent an embellishment of the piston-only, segmented corrector in which 2 additional degrees of freedom (tip and tilt) are added for slope control. This results in improved wavefront fitting and reduced number of segments needed to achieve the same level of correction (Fig. 2, bottom).

Each of the wavefront correctors was modeled as a square grid of equally spaced and independently controlled actuators or segments, with essentially infinite resolution. While in practice, the resolution is limited by the bit depth of the control electronics (typically 8–14 bits), our modeling revealed little performance advantage with unlimited resolution. The dynamic range (stroke) of the actuators was not constrained, assuring the range was always larger than the PV errors in the two populations.

The surface shape for all three wavefront correctors, $\phi_{cor}(x, y)$, can be predicted principally from the maximum surface deflection of each actuator, A_n, the influence function of each actuator $g_n(x, y)$, and their interdependency. A common approach, chosen here due to the large number of corrector variations evaluated, is to assume identical and independent influence functions [46,47]. This results in linearity of the actuator responses and permits modeling the corrector surface with the following relationship:

$$\varphi_{cor}(x,y)=\sum_{n=1}^{N}A_n g_n(x - x_n, y - y_n),$$

(1)

where N is the total number of actuators, x and y are spatial coordinates at the corrector, and x_n and y_n define the center location of the nth actuator. While our neglect of the interdependency of the actuators precludes capturing some performance aspects of real correctors, it provides reasonable performance estimates for correctors that one might consider for a vision AO system. The influence function, $g_n(x, y)$, uniquely distinguishes the three correctors, Eq. (1).

For discrete actuator DMs, the influence function can be approximated as a Gaussian, i.e.,

$$g_n(x,y)=\exp\left(\frac{-(x - x_n)^2}{2\sigma^2}\right)\exp\left(\frac{-(y - y_n)^2}{2\sigma^2}\right),$$

(2)

where σ defines the spatial extent of the influence function. In our model, σ was set to give a coupling coefficient of 12%, an approximate value for many discrete actuator DMs [23,37]. The linear relationship of Eq. (1) predicts a slightly rippled surface when all of the actuators are displaced by the same amount. This pinning error [25], does not occur in actual DMs that have stiff faceplates and does give an underestimate of actual device performance.

The influence function for piston-only segmented correctors was modeled as a top hat having a constant value across each individual segment (which is controlled by a single actuator) and zero across all other segments. The gaps between the square segments were assumed to be zero (100% fill factor). The mirror performance with other fill factors can be found in Miller *et al.* [42].

Piston/tip/tilt, segmented correctors were modeled with 3 degrees of freedom per segment, with each having its own independent influence function. The gaps between the square segments were again assumed to be zero. In practice, fill factors of 96%–99% can be routinely achieved [48].

Performance for the three corrector types was determined using the following procedure:

1. An influence function matrix, I_{cor}, is generated for a specific corrector type and number of actuators, N, as given by Eq. (3). Edge effects of the circular pupil were accounted for in the individual influence functions. I_{cor} represents a P by N matrix in

which each column corresponds to the influence function, $g_n(x, y)$, of a single actuator. P is the total number of sampling points across the influence function profile in the circular aperture. For piston/tip/tilt, segmented correctors, each column in Eq. (3) contains three influence functions that describe one segment:

$$I_{cor} = \begin{bmatrix} I(1,1) & I(1,2) & \ldots & \ldots & I(1,N) \\ I(2,1) & I(2,2) & \ldots & \ldots & I(2,N) \\ \ldots & \ldots & \ldots & \ldots & \ldots \\ \ldots & \ldots & \ldots & \ldots & \ldots \\ I(P,1) & I(P,2) & \ldots & \ldots & I(P,N) \end{bmatrix}. \tag{3}$$

2. A wavefront aberration map, ϕ_{eye}, is reconstructed using the measured Zernike coefficients from the Shack–Hartmann aberrometry for a specific pupil size and eye in the two populations.

3. Singular value decomposition is used to invert the influence function matrix (step 1) I_{cor}^-. I_{cor}^- and the wavefront aberrations of the eye (step 2) are inserted into Eq. (4). The actuator deflections, A_n, are then determined by solving

$$A_n = I_{cor}^- \varphi_{eye}, \tag{4}$$

where A_n and ϕ_{eye} are column matrices described by

$$A_n = \begin{bmatrix} A_1 \\ A_2 \\ \ldots \\ \ldots \\ A_N \end{bmatrix} \quad \varphi_{eye} = \begin{bmatrix} \varphi_1 \\ \varphi_2 \\ \ldots \\ \ldots \\ \varphi_P \end{bmatrix}. \tag{5}$$

This approach produces values for A_n that minimize the rms residual wavefront error

4. The corrector surface, ϕ_{cor}, is reconstructed from the actuator deflections, A_n, and then subtracted from the wavefront aberration of the eye, ϕ_{eye}. The resulting residual aberration is $\phi_{residual}$.

5. The complex field, ψ, at the pupil is represented as $|\psi| \exp(ik\phi_{residual})$ with the amplitude of the wavefront, $|\psi|$, defined as unity inside and zero outside of the circular pupil. k is equal to $2\pi/\lambda$ with λ being the wavelength of light. Fourier transforming ψ and taking its squared modulus yields the corrected point-spread function (PSF). Thus the PSF includes the impact of residual aberrations and scalar diffraction effects generated by the finite size of the pupil. The Strehl ratio was used as the figure of merit and is defined as the ratio of the light intensity at the peak of the aberrated PSF to that at the peak of the aberration-free PSF. Generally, an optical system is considered diffraction limited if the Strehl is ≥ 0.8.

Other common figures of merit include root-mean-square (rms) wavefront error and full width at half-height (FWHH) of the PSF. For reasonably well-corrected systems, however, the rms and FWHH generally provide little additional information about image quality beyond that revealed by Strehl. This is because for such systems, Strehl and rms are highly correlated [49], while the FWHH of the PSF is largely insensitive to small changes in the wave aberrations, which Strehl is not. As such, Strehl is a

reliable guide for establishing corrector requirements for diffraction-limited imaging in the human eye and is therefore used here.

6. Steps 1 through 5 are repeated for each corrector type, actuator number, pupil diameter (4.5, 6, 7.5 mm), wavelength (0.4, 0.6, 0.8, and 1.0 μm), and for each eye in the two populations.

This procedure is illustrated in Fig. 3 for the compensation of aberrations across a 7.5 mm pupil using a discrete actuator DM, piston-only segmented corrector, and piston/tip/tilt segmented corrector. Each corrector has seven actuators or segments across the pupil diameter. Figure 3 (a) is the measured uncorrected wave aberration for a single subject from the Rochester population with defocus zeroed. Figures 3(b), 3(e), and 3(h) show the respective conjugate mirror surface that minimizes the rms wavefront error for each of the mirror types. Figures 3 (c), 3(f), and 3(i) show the residual error after correction of the wave aberrations in Fig. 3(a). The corresponding corrected point spread functions and Strehl ratios are given in Figures 3(d), 3(g), and 3(j) for a wavelength, $\lambda = 0.6$ μm. It should be noted that the segmented piston/tip/ tilt device has three actuators per segment compared with just one for the other two devices.

3. Results

A. Required Corrector Stroke for the Two Populations

Regardless of corrector type and number of actuators, effective compensation requires the dynamic range of the corrector to be at least equal to the peak-to-valley (PV) error of the aberrations (assuming no phase wrapping). For reflective correctors, this means the maximum physical excursion of their reflective surface must be at least one-half of the PV error.

Figure 4 shows the PV wavefront error that encompasses 25%, 50%, and 95% of the two populations for 4.5–7.5 mm pupils. In each plot, three curves are shown for each population and correspond to the three different second-order states. As expected, the PV error increases monotonically with increasing pupil size. Note the second-order aberrations in the Rochester population include the subject's entire refractive error, while the Indiana data include only the residual error after a subjective refraction. This inherent difference makes a direct comparison of the two datasets difficult as higher-order aberrations influence the patient's best subjective refraction and lead to nonzero residual defocus and astigmatism. Zeroing Zernike coefficients (as was done for four of the six curves in each of the Fig. 4 plots) is, therefore, not directly equivalent to an ideal conventional refraction and can lead to higher PV errors.

In Fig. 4, the PV error noticeably increases with the addition of the second-order terms and is consistently larger for the Rochester population for all three-second-order states. The PV error for a 7.5 mm pupil that encompassed 95% of the Rochester population was 53, 18, and 10 μm for the three second-order conditions. For the Indiana population, the corresponding 95% errors were 11, 10, and 7 μm. The largest errors of 53 μm (Rochester) and 11 μm (Indiana) depict the most demanding conditions for the corrector. For comparison, Xinetics type DMs employed in some vision science cameras [1,2,6,7,9,11] have a stroke of only 4 μm (8 μm in wavefront after reflection), which approaches the 11 μm (Indiana data) required to correct for the patient's residual defocus and astigmatism and higher-order aberrations but falls considerably short of the 53 μm (Rochester data) needed to correct for all of the patient's defocus, astigmatism, and higher-order aberrations.

B. Required Actuator Number for Discrete Actuator Deformable Mirrors

Figure 5 (top) shows the predicted mean corrected Strehl for discrete actuator DMs as a function of the number of actuators (7.5 mm pupil, $\lambda = 0.6$ μm). The six curves cover the two populations and the three different levels of second-order aberration defined previously. One curve includes

representative error bars that correspond to ±1 standard deviation across the population. All curves exhibit a similar shape that is monotonic and positively sloped. With zero actuators, the corrected Strehl reflects the image quality of the eye without wavefront correction. For five to nine actuators across the pupil, the Strehl ratio for five of the six curves rises sharply, indicating a significant improvement in image quality, small changes in the number of actuators leading to noticeable changes in corrected image quality. This increase is due to the effective correction of the lower-order aberrations, which contain the largest percentage of the wave aberration variance [44,50]. The error bars are relatively large over this range, reflecting the large variability in corrector performance between the worst and best eyes. For more than nine actuators across the pupil, the Strehl ratio rises gradually to an asymptotic value of 1. The diminishing improvement in corrected image quality makes larger and more expensive correctors increasingly less attractive.

For the Indiana population, 11–14 actuators across the 7.5 mm pupil diameter are required to achieve a Strehl ratio ≥0.8. The actual number depends on the magnitude of the second-order terms in the wave aberration. For the Rochester population, with a larger average aberration magnitude, 14 to 15 actuators across the pupil were required for the two cases where second-order defocus and astigmatism (Z3–Z5) and second-order defocus (Z4) were zeroed prior to correction. The most aberrated scenario, which included all second-order terms, clearly required many more actuators than the largest considered here (21 across the pupil), which only increased the Strehl to 0.18.

Figure 5 (middle) and (bottom) show the predicted mean corrected Strehl for smaller pupils of 6 and 4.5 mm, respectively. In the Rochester population, decreasing the pupil size to 6 mm reduces the number of actuators across the pupil for diffraction-limited imaging to approximately 9. For the Indiana population, the corresponding actuator numbers are 7 and 8. For the 4.5 mm pupil, the numbers are 6 to 7 and 4 to 5 for the Rochester and Indiana populations, respectively.

Figure 6 shows the correction performance at four wavelengths (0.4, 0.6, 0.8, and 1.0 μm) that span the visible and near-infrared spectra, the wavelengths most relevant to retinal imaging and obviously vision. Results are for the specific case of a 7.5 mm pupil and zeroed defocus in the Indiana study. Results for other cases can be extrapolated based on the trends present in Fig. 6. The correction is highly dependent on wavelength; for seven actuators across the pupil, the corrected Strehl in Fig. 6 varies from 0.2 (0.4 μm) to 0.64 (1 μm). Correction at shorter wavelengths requires noticeably more actuators than at longer wavelengths to achieve the same imaging performance. Further discussion of the wavelength impact can be found in Miller *et al.* [42].

C. Required Actuator Number for Piston-Only, Segmented Correctors

Figure 7 shows the predicted corrected Strehl for piston-only, segmented correctors as a function of the number of actuators ($\lambda = 0.6$ μm) for 7.5 (top), 6 (middle), and 4.5 mm (bottom) pupils. Each contains six curves that cover the two populations and the three levels of second-order aberration. One of the six includes representative error bars of ±1 standard deviation across the population. While the general trend of the curves is similar to that for the discrete actuator DMs, the number of required segments is much higher to achieve the same imaging performance.

For example, in the Indiana population (7.5 mm pupil), 50–90 segments across the pupil diameter are required to achieve a Strehl ratio ≥0.8, with the actual number being highly sensitive to the magnitude of the second-order aberrations. A 90×90 piston-only, segmented corrector gives the same corrected Strehl (0.8) as a discrete actuator DM with 14×14 actuators. For the Rochester population, 95–115 segments are required to reach a Strehl ratio of 0.8 if

defocus and astigmatism (Z3–Z5) or defocus alone (Z4) were zeroed prior to correction. Even the largest segmented mirror considered in our study (150 × 150 actuators) performed poorly when attempting to correct all of the second- and higher-order aberrations, just reaching a Strehl of 0.2.

For the smaller pupil diameters, the required number of actuators decreases accordingly. For 6 mm, the required number of segments to achieve diffraction-limited imaging are 40–55 and 25–40 segments for the Rochester and Indiana populations, respectively. For 4.5 mm, the values are 10–15 segments and 15–25 segments, respectively. The values for the Rochester population do not include the case where all aberrations are present.

D. Required Actuator Number for Piston/tip/tilt, Segmented Correctors

Figure 8 shows the predicted Strehl performance for piston/tip/tilt, segmented correctors under the same conditions used for the previous two mirror types (Figs. 5 and 7). For the Rochester population, 12 segments reach a Strehl ratio of 0.8 if defocus and astigmatism (Z3–Z5) or defocus alone (Z4) were zeroed prior to correction. A Strehl ratio of 0.8 can be reached with just 19 actuators across the pupil if all of the second-order terms are present. For the piston-only, segmented devices described in Subsection 3.C, even 150 actuators across the pupil is insufficient. For the Indiana population, 9 to 10 segments across the diameter are required for a Strehl of 0.8, with the number being insensitive to the magnitude of the second-order aberrations.

Like the other wavefront correctors, for smaller pupil diameters, the required number of actuators decreases accordingly. For 6 mm, the required number of segments to achieve diffraction-limited imaging are 8–13 and approximately 6 segments for the Rochester and Indiana populations, respectively. For 4.5 mm, the values are 5 to 9 and 3 to 4 segments, respectively. The values for the Rochester population do not include the case where all aberrations are present.

The addition of tip and tilt control clearly improves the wavefront fitting, especially at the edges of the pupil where the slopes can be great. This comes at the expense of additional complexity in mirror control in that three movement controls are required for each segment rather than one.

4. Discussion

The performance of three general wavefront corrector types was systematically evaluated as a function of pupil size, second-order aberration state, imaging wavelength, and actuator number. Actuator influence function was representative of that typical for each of the corrector types. In this way, the analysis retained its generality, making it applicable to a wide variety of available commercial wavefront correctors as well as new ones in the future. To simplify the analysis, the actuator response was assumed to be linear. Actuator stroke and number required for achieving a specific performance level were independently determined by basing the first solely on the PV errors of the two populations and the second assuming a stroke larger than the PV error. While this approach does not cover device configurations in which actuator stroke and number simultaneously limit performance, it does establish lower bounds on the requirements for the two actuator parameters.

A. Required Actuator Stroke

Regardless of corrector type, effective compensation requires the dynamic range of the corrector to be at least equal to the PV error of the aberrations. For reflective correctors, this means the maximum physical excursion of their reflective surface must be at least one-half of

the PV error. For segmented correctors (either reflective or transmissive), the stroke can be effectively increased with phase wrapping, though limitations apply [38,42].

The PV errors in Fig. 4 correspond to extreme wavefront deviations that could have occurred anywhere in the pupil, including immediately next to each other. Quantification of this spatial separation in the two populations, which we did not do, would have provided a more complete description of the PV error and placed requirements on the interactuator stroke in addition to that for the full stroke, which we did evaluate. The interactuator stroke corresponds to the maximum displacement between two adjacent actuators and is always less than or equal to the full stroke. Full stroke is defined as the maximum range over which all of the actuators can move collectively, i.e., simultaneously applied with the same driving voltage. Our analysis can be extended to include interactuator stroke requirements. However, when there are sufficient actuators to produce a good correction, the wavefront aberrations in the two populations become relatively smooth compared with the spacing of actuators. This suggests that the global stroke, rather than the interactuator stroke, is more critical in assessing stroke requirements.

Most commercial wavefront correctors have insufficient stroke to traverse the PV errors shown in Fig. 4 for large pupils. However, there are several strategies for reducing the error to a more manageable level. For retinal imaging applications, a possible strategy is to minimize PV errors by meticulously employing trial lenses in conjunction with continuously adjustable lenses to optimize retinal image quality and to avoid quantization errors of the trial lenses [1]. Another approach is to cascade a large stroke, low fidelity corrector (e.g., bimorph DM) to correct the relatively large second-order aberrations and a smaller stroke, high fidelity corrector (e.g., a MEMS DM) to compensate for higher-order aberrations [51]. Double pass schemes have also been proposed [52]. Finally, some retinal imaging and vision applications have less demanding resolution requirements and therefore can operate with smaller pupils. For example, reducing the 7.5 mm pupil size to 6 and 4.5 mm in the Rochester population reduces the PV error to 30, 10, and 5 μm and 17, 7, and 3 μm, respectively for the three second-order states. For the Indiana population, the corresponding PV error reduces to 6, 5, and 4 μm and 2.5, 2, and 1.5 μm.

B. Required Actuator Number

1. Discrete Actuator Deformable Mirror—Discrete actuator DMs were modeled using a linear superposition of Gaussian influence functions. While easy to conceptualize, the assumption of linearity likely underestimates the fitting performance, an error that increases with the aberrations. Hence, the model probably underestimated the corrector performance somewhat more for the Rochester population than for the Indiana population, especially for the highly aberrated case in which there was no defocus and astigmatism correction (Fig. 5). This effect can be eliminated by use of a more accurate model, for example, finite-element analysis (FEA) [53], that incorporates the material properties of the corrector such as thickness, modulus of elasticity, and Poisson's ratio that determine the influence functions and ultimately mirror shape [54-56]. Such analysis, however, must be customized for a particular wavefront corrector, an approach not readily applicable for the many corrector configurations evaluated here. A more plausible use of FEA would be to fine-tune the performance of specific correctors that were found to perform well with the linear model.

Performance predictions with our linear model roughly agree with experimental results reported in the literature. For example, Xinetics DMs totaling 37 (7 across) [1,2,6,9,11,13] and 97 actuators (11 across) [57] actuators have been employed in several AO systems for vision science. Using Fig. 5 (middle), the 37 actuator Xinetics is predicted to increase the Strehl from 0.03 to 0.5 for the Rochester population with zeroed defocus for a 6 mm pupil. In comparison, Hofer *et al.* [2] used the same corrector to achieve a dynamically corrected Strehl ratio of 0.34 ± 0.12 for a 6 mm pupil at 0.55 μm wavelength after a trial lens refraction (average of six subjects). While the 0.34 Strehl is lower than the predicted 0.5, this discrepancy might be

explained by a number of differences. First, there is a wavelength difference, 0.55 μm instead of 0.6 μm. Second, the experimental correction was applied over a 6.8 mm pupil with the central 6 mm (the model used 6 mm) providing the wavefront measurement. Both differences will cause a reduction in the experimental Strehl. Roorda *et al.* [9] report corrected rms values as low as 0.09 μm for a 7 mm pupil, giving predicted Strehls of up to 0.34. Similarly, Rha *et al.* [6] give corrected rms values of 0.07 μm for a 6.8 mm pupil, giving Strehls of 0.52. Both systems employ a 37 channel Xinetics DM.

2. Segmented Piston-Only, and Piston/tip/tilt Correctors—Segmented piston-only correctors rely on local piston correction to remove aberrations and therefore require a minimum of two segments to correct for wavefront slope. It is not surprising then that these correctors require many more actuators than the discrete actuator DMs described previously. The study reported by Miller *et al.* [42] found that 48 piston-only segments were required for diffraction-limited imaging across a 6 mm pupil in 0.6 μm light. For this scenario, residual defocus and astigmatism (Z3–Z5) was present after a conventional refraction. The requirement was reduced to 20 segments when the second-order terms were completely removed prior to correction. Our results with the Indiana population agree well with this study, finding that for a 6 mm pupil, the required number of segments to achieve diffraction-limited imaging is 25–40 segments. For the Rochester population, which unlike the other studies did not include a subjective refractive, the required number of segments was higher (40–55).

The 2 extra degrees of freedom of the segmented piston/tip/tilt mirrors provide wavefront slope correction and therefore drastically reduce the required number of segments. The added degrees of freedom, however, add complexity and may be one of the reasons why few such correctors have been made, and none have yet to be applied to the human eye.

Segmented piston-only and piston/tip/tilt correctors were modeled having 100% fill (no gaps). In reality, fill coverage of 96%–99% is typical [48] and can diffract incident light away from the core of the point spread. For these fills, however, the effect should be small if they follow the trend reported by Miller *et al.* [42], who quantified the drop in Strehl for fills of 73.5% and 86%. For example, Miller *et al.* [42] showed for a particular configuration that the mean Strehl dropped by 0.22 (from 0.9 to 0.68) and 0.4 (from 0.9 to 0.5) when the fill coverage decreased from 100% to 86% and 73.5%, respectively. For the segmented piston/tip/tilt correctors, edge effects at the gaps due to tilting of the segments were assumed negligible.

3. Phase Wrapping—A unique advantage of segmented correctors, in principle, is their ability to correct large PV errors using a limited stroke of just 2π rad. The segmented nature permits abrupt changes in the phase profile required to phase wrap to modulo 2π. Most LC-SLMs are purposely designed for 2π phase correction and rely on phase wrapping to extend their dynamic range [38,42]. A fundamental weakness is the system can only correct at a single wavelength and its associated harmonics. The results in Figs. 7 and 8 represent both unwrapped and wrapped devices, but correct interpretation of the latter is contingent on perfect 2π wrapping at the one wavelength.

The effects of phase wrapping for correcting the aberrations of the eye in polychromatic light have been explored by Miller *et al.* [42]. Their model included the impact of the dispersion of the liquid crystal material (E-7) and the longitudinal chromatic aberrations of the normal eye. The impact of the eye's intrinsic longitudinal chromatic aberrations was shown to be significantly more degrading than either phase wrapping or material dispersion.

C. Dynamic Versus Static Correction

Studies have shown that temporal fluctuations in the wave aberrations of the eye range from 1 to 12 Hz, with most of the energy confined below 1 Hz [26,27]. Contributing to this are the

microfluctuations in accommodation that can typically vary the defocus coefficient by ~0.1 μm [26]. Ocular temporal fluctuations are well within the bandwidth of essentially all wavefront correctors, with the exception of those based on liquid crystals. As such, a static treatment of the aberrations, as was chosen for our analysis, is sufficient for capturing the performance of most wavefront correctors. A particular advantage of segmented correctors, however, is given zero or negligible hysteresis and interactuator coupling; they allow open loop operation, i.e., no feedback control.

D. Required Parameters

Table 1 summarizes the results for the three wavefront corrector types analyzed for actuator stroke and number for a 7.5 mm pupil. Also listed are corrector specifications for temporal bandwidth, reflectivity, and corrector size, which are also important for retinal imaging and vision application. High mirror reflectivity (>90%) assures high throughput efficiency of the corrector, particularly critical for retinal imaging applications in which a hard upper limit exists for the amount of light that can be safely directed into the human eye. A corrector size comparable with a dilated pupil (~7–8 mm) permits the use of short focal length lenses and mirrors, and facilitates compact system designs. The required corrector stroke was observed to vary with the population as well as the second-order aberration condition, with values ranging from 10 to 53 μm (Rochester data) and 7 to 11 μm (Indiana data). The required number of mirror actuators also varied depending on the population, the second-order aberration condition, and mirror type.

5. Conclusion

The extent to which AO can effectively improve resolution and contrast fundamentally depends on its ability to accurately measure, track, and correct ocular aberrations. As surveyed, numerous types of wavefront correctors have been applied to the eye, yet none have reported diffraction-limited imaging for large pupils (≥6 mm). This raises a fundamental concern as to the required characteristics of a correcting device to achieve diffraction-limited imaging and to optimally match corrector performance and cost to that required of a particular imaging task in the eye.

Our analysis represents a first attempt at exploring the most critical parameters for three general types of correctors. A more detailed assessment that accounts for variations in the actuator influence functions, the magnitude of the actuator coupling coefficient, and the interdependency and distribution of the actuators will lead to improved quantitative predictions of corrector performance, especially when implemented in the context of finite-element analysis.

In conclusion, correction of the wave aberration of the eye remains challenging, especially for diffraction-limited imaging through large pupils. Understanding the performance parameters that enable such imaging in the population at large will guide new, compact correctors and lead to more effective research and commercial instruments for retinal imaging and vision testing.

Acknowledgements

References

1. Liang J, Williams DR, Miller DT. Supernormal vision and high-resolution retinal imaging through adaptive optics. J Opt Soc Am A 1997;14:2884–2892.

2. Hofer H, Chen L, Yoon GY, Singer B, Yamauchi Y, Williams DR. Improvement in retinal image quality with dynamic correction of the eye's aberrations. Opt Express 2001;8:631–643.

3. Larichev V, Ivanov PV, Iroshnikov NG, Shmalhauzen VI, Otten LJ. Adaptive system for eye-fundus imaging. Quantum Electron 2002;32:902–908.

4. Ling N, Zhang Y, Rao X, Li X, Wang C, Hu Y, Jiang W. Small table-top adaptive optical systems for human retinal imaging. Proc SPIE 2002;4825:99–108.

5. Glanc M, Gendron E, Lacombe F, Lafaille D, Le Gargasson JF, Lena P. Towards wide-field imaging with adaptive optics. Opt Commun 2004;230:225–238.

6. Rha J, Jonnal RS, Thorn KE, Qu J, Zhang Y, Miller DT. Adaptive optics flood-illumination camera for high speed retinal imaging. Opt Express 2006;14:4552–4569.

7. Choi SS, Doble N, Hardy JL, Jones SM, Keltner JL, Olivier SS, Werner JS. *In vivo* imaging of the photo-receptor mosaic in retinal dystrophies and correlations with retinal function. Invest Ophthalmol Visual Sci 2006;47:2080–2092. [PubMed: 16639019]

8. Dreher AW, Bille JF, Weinreb RN. Active optical depth resolution improvement of the laser tomographic scanner. Appl Opt 1989;28:804–808.

9. Roorda A, Romero-Borja F, Donnelly WJ, Queener H, Hebert TJ, Campbell MCW. Adaptive optics scanning laser ophthalmoscopy. Opt Express 2002;10:405–412.

10. Hammer DX, Ferguson RD, Bigelow CE, Iftimia NV, Ustun TE, Burns SA. Adaptive optics scanning laser ophthalmoscope for stabilized retinal imaging. Opt Express 2006;8:3354–3367.

11. Miller DT, Qu J, Jonnal RS, Thorn K. Coherence gating and adaptive optics in the eye. Proc SPIE 2003;4956:65–72.

12. Hermann B, Fernandez EJ, Unterhuber A, Sattmann H, Fercher AF, Drexler W, Prieto PM, Artal P. Adaptive-optics ultrahigh-resolution optical coherence tomography. Opt Lett 2004;29:2142–2144. [PubMed: 15460883]

13. Zhang Y, Rha J, Jonnal RS, Miller DT. Adaptive optics parallel spectral domain optical coherence tomography for imaging the living retina. Opt Express 2005;13:4792–4811.

14. Zawadzki RJ, Jones S, Olivier SS, Zhao M, Bower BA, Izatt JA, Choi SS, Laut S, Werner JS. Adaptive-optics optical coherence tomography for high-resolution and high-speed 3D retinal *in vivo* imaging. Opt Express 2005;13:8532–8546. [PubMed: 19096728]

15. Zhang Y, Cense B, Rha J, Jonnal RS, Gao W, Zawadzki RJ, Werner JS, Jones S, Olivier S, Miller DT. High-speed volumetric imaging of cone photoreceptors with adaptive optics spectral-domain optical coherence tomography. Opt Express 2006;14:4380–4394. [PubMed: 19096730]

16. Fernández EJ, Považvay B, Hermann B, Unterhuber A, Sattmann H, Prieto PM, Leitgeb R, Ahnelt P, Artal P, Drexler W. Three-dimensional adaptive optics ultrahigh-resolution optical coherence tomography using a liquid crystal spatial light modulator. Vision Res 2005;45:3432–3444. [PubMed: 16249013]

17. Merino D, Dainty C, Bradu A, Podoleanu AG. Adaptive optics enhanced simultaneous *en-face* optical coherence tomography and scanning laser ophthalmoscopy. Opt Express 2006;8:3345–3353.

18. Yoon GY, Williams DR. Visual performance after correcting the monochromatic and chromatic aberrations of the eye. J Opt Soc Am A 2002;19:266–275.

19. Artal P, Chen L, Fernández EJ, Singer B, Manzanera S, Williams DR. Neural compensation for the eye's optical aberrations. J Vision 2004;4:281–287.

20. Chen L, Kruger PB, Hofer H, Singer B, Williams DR. Accommodation with higher-order monochromatic aberrations corrected with adaptive optics. J Opt Soc Am A 2006;23:1–8.

21. Porter, J.; Queener, H.; Lin, J.; Thorn, K.; Awwal, AAS., editors. Adaptive Optics for Vision Science: Principles, Practices, Design and Applications. Wiley; 2006.

22. Doble N. High-resolution, *in vivo* retinal imaging using adaptive optics and its future role in ophthalmology. Expert Rev Medical Devices 2005;2:205–216.
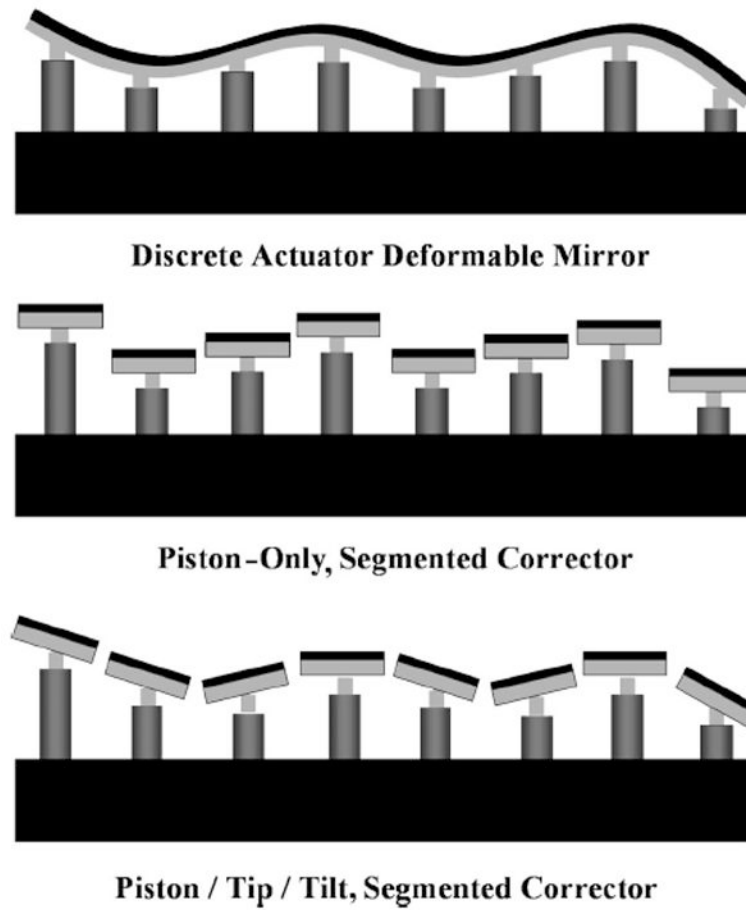
23. Oppenheimer BR, Palmer DL, Dekany RG, Sivaramakrishnan A, Ealey MA, Price TR. Investigating a Xinetics Inc. deformable mirror. Proc SPIE 1997;3126:569–579.

24. Hardy, JW. Adaptive Optics for Astronomical Telescopes. Oxford U. Press; 1998.

25. Tyson, RK. Principles of Adaptive Optics. Vol. 2. Academic; 1998.

26. Hofer H, Artal P, Singer B, Aragon JL, Williams DR. Dynamics of the eye's wave aberration. J Opt Soc Am A 2001;18:497–506.

27. Diaz-Santana L, Torti C, Munro I, Gasson P, Dainty C. Benefit of higher closed-loop bandwidths in ocular adaptive optics. Opt Express 2003;11:2597–2605.

28. Burns SA, Marcos S, Elsner AE, Bara S. Contrast improvement for confocal retinal imaging using phase correcting plates. Opt Lett 2002;27:400–402. [PubMed: 18007814]

29. Fernandez EJ, Vabre L, Hermann B, Unterhuber A, Povazay B, Drexler W. Adaptive optics with a magnetic deformable mirror: applications in the human eye. Opt Express 2006;14:8900–8917.

30. Doble N, Williams DR. The application of MEMS technology for adaptive optics in vision science. IEEE J Sel Top Quantum Electron 2004;10:629–635.

31. Vdovin GV, Sarro PM. Flexible mirror micromachined in silicon. Appl Opt 1995;34:2968–2972.

32. Fernandez EJ, Artal P. Membrane deformable mirror for adaptive optics: performance limits in visual optics. Opt Express 2003;11:1056–1069.

33. Fernandez EJ, Iglesias I, Artal P. Closed-loop adaptive optics in the human eye. Opt Lett 2001;26:746–748. [PubMed: 18040440]

34. Bartsch D-U, Zhu L, Sun PC, Fainman S, Freeman WR. Retinal imaging with a low-cost micromachined membrane deformable mirror. J Biomedical Opt 2002;7:451–456.

35. Dalimier E, Dainty C. Comparative analysis of deformable mirrors for ocular adaptive optics. Opt Express 2005;13:4275–4285.

36. Doble N, Yoon G, Chen L, Bierden P, Singer B, Olivier S, Williams DR. The use of a microelectromechanical mirror for adaptive optics in the human eye. Opt Lett 2002;27:1579–1581.

37. Perreault JA, Bifano TG, Levine BM, Horenstein MN. Adaptive optic correction using microelectromechanical deformable mirrors. Opt Eng 2002;41:561–566.

38. Thibos LN, Bradley A. Use of liquid-crystal adaptive-optics to alter the refractive state of the eye. Optom Vision Sci 1997;74:581–587.

39. Vargas-Martin F, Prieto PM, Artal P. Correction of the aberrations in the human eye with a liquid-crystal spatial light modulator: limits to performance. J Opt Soc Am A 1998;15:2552–2562.

40. Prieto PM, Fernandez EJ, Manzanera S, Artal P. Adaptive optics with a programmable phase modulator: applications in the human eye. Opt Express 2004;12:4059–4071.

41. Li FH, Mukohzaka N, Yoshida N, Igasaki Y, Toyoda H, Inoue T, Kobayashi Y, Hara T. Phase modulation characteristics analysis of optically-addressed parallel-aligned nematic liquid crystal phase-only spatial light modulator combined with a liquid crystal display. Opt Rev 1998;5:174–178.

42. Miller DT, Thibos LN, Hong X. Requirements for segmented correctors for diffraction-limited performance in the human eye. Opt Express 2005;13:275–289.

43. Thibos LN, Applegate RA, Schwiegerling JT, Webb R. VISA Standards Taskforce Members. Standards for reporting the optical aberrations of eyes. J Refract Surg 2002;18:S652–S660. [PubMed: 12361175]

44. Thibos LN, Hong X, Bradley A, Cheng X. Statistical variation of aberration structure and image quality in a normal population of healthy eyes. J Opt Soc Am A 2002;19:2329–2348.

45. He JC, Marcos S, Webb RH, Burns SA. Measurement of the wave-front aberration of the eye by a fast psychophysical procedure. J Opt Soc Am A 1998;15:2449–2456.

46. Hudgin RH. Wave-front compensation error due to finite element corrector size. J Opt Soc Am 1977;67:393–395.

47. Roggemann, MC.; Welsh, B. Imaging Through Turbulence. CRC; 1996.

48. Doble N, Helmbrecht M, Hart M, Juneau T. Advanced wave-front correction technology for the next generation of adaptive optics equipped ophthalmic instrumentation. Proc SPIE 2006;5688:125–132.

49. King WB. Dependence of the Strehl ratio on the magnitude of the variance of the wave aberration. J Opt Soc Am 1967;58:655–661.

50. Porter J, Guirao A, Cox IG, Williams DR. Monochromatic aberrations of the human eye in a large population. J Opt Soc Am A 2001;18:1793–1803.

51. Zawadzki, RJ.; Choi, SS.; Werner, JS.; Jones, SM.; Chen, D.; Olivier, SS.; Zhang, Y.; Rha, J.; Cense, B.; Miller, DT. Two deformable mirror adaptive optics system for *in vivo* retinal imaging with optical coherence tomography. presented at the 2006 Biomedical Optics Topical Meeting; Fort Lauderdale, Fla., USA. 22 March 2006;

52. Webb RH, Albanese MJ, Zhou Y, Bifano T, Burns SA. Stroke amplifier for deformable mirrors. Appl Opt 2004;43:5330–5333. [PubMed: 15495423]

53. Zienkiewicz, OC. The Finite Element Method in Engineering Science. Vol. 2. McGraw-Hill; 1971.

54. Lee JH, Uhm T-K, Youn S-K. First-order analysis of thin-plate deformable mirrors. J Korean Phys Soc 2004;44:1412–1416.

55. Arnold L. Influence functions of a thin shallow meniscus-shaped mirror. Appl Opt 1997;36:2019–2028. [PubMed: 18253168]

56. Menikoff A. Actuator influence functions of active mirrors. Appl Opt 1991;30:833–838.

57. Putnam NM, Hofer HJ, Doble N, Chen L, Carroll J, Williams DR. The locus of fixation and the foveal cone mosaic. J Vision 2005;5:632–639.
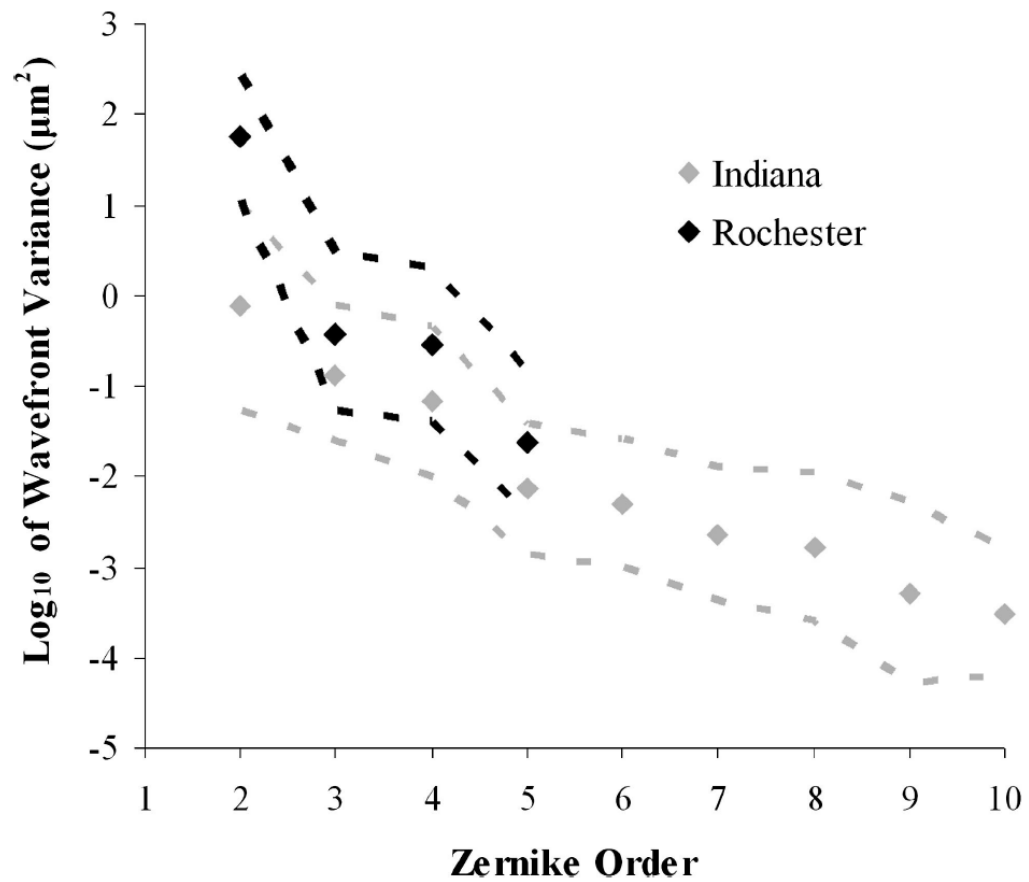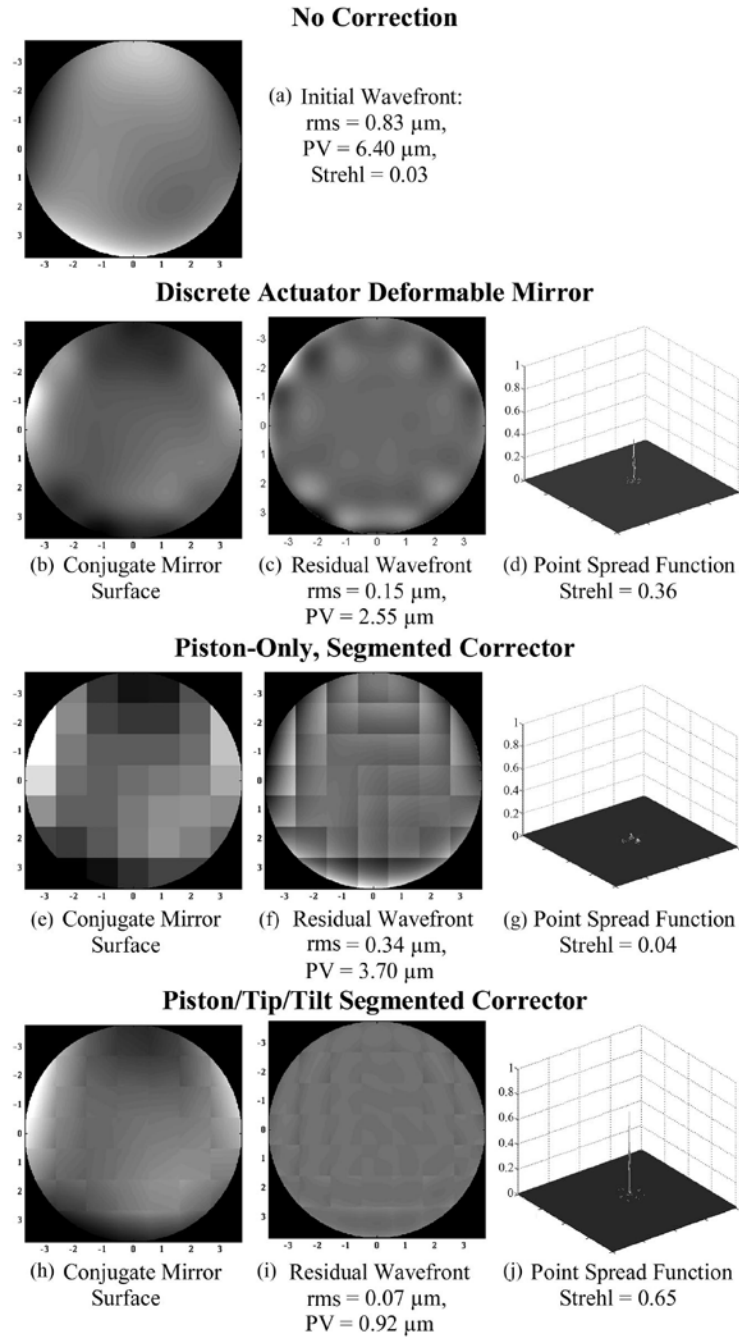
Fig. 1.
Log_{10} of the wavefront variance plotted as a function of Zernike order for the two populations (7.5 mm pupil). Diamonds and corresponding dashed curves represent the mean and mean ± 2 times the standard deviation of the log_{10} (wavefront variance), respectively, for the 70 eyes measured in the Rochester (black) and Indiana (gray) studies.

Discrete Actuator Deformable Mirror

Piston–Only, Segmented Corrector

Piston / Tip / Tilt, Segmented Corrector

Fig. 2.
Schematic cross sections of the three types of wavefront correctors evaluated. For illustration, the reflective surface of each corrector is configured for compensating the same wavefront aberration. See text for description of the corrector types.

No Correction

(a) Initial Wavefront:
rms = 0.83 μm,
PV = 6.40 μm,
Strehl = 0.03

Discrete Actuator Deformable Mirror

(b) Conjugate Mirror
Surface

(c) Residual Wavefront
rms = 0.15 μm,
PV = 2.55 μm

(d) Point Spread Function
Strehl = 0.36

Piston-Only, Segmented Corrector

(e) Conjugate Mirror
Surface

(f) Residual Wavefront
rms = 0.34 μm,
PV = 3.70 μm

(g) Point Spread Function
Strehl = 0.04

Piston/Tip/Tilt Segmented Corrector

(h) Conjugate Mirror
Surface

(i) Residual Wavefront
rms = 0.07 μm,
PV = 0.92 μm

(j) Point Spread Function
Strehl = 0.65

Fig. 3.
Compensation of aberrations across a 7.5 mm pupil using a discrete actuator DM, piston-only, and piston/tip/tilt segmented correctors. Each of the mirrors has seven actuators or segments across the pupil diameter. Wavefront phase is represented by a gray-scale image (black and white tones depict minimum and maximum phase, respectively). (a) Measured uncorrected wave aberration for one subject's eye from the Rochester population with defocus zeroed. (b) Conjugate mirror surface that minimizes the rms wavefront error for the subject's wave aberrations in (a) for the discrete actuator device. (c) Residual aberrations after correction of the wave aberrations in (a) with the corrector phase profile in (b). The phase rms and PV are specified at the bottom of each image. The corresponding corrected point spread function and

Strehl ratio is given in (d), with the former computed using scalar diffraction theory that incorporated the residual wave aberration and a circular pupil ($\lambda = 0.6$ μm). (e)–(g) Mirror phase profile, residual aberrations, and the corrected point spread for the piston-only case, respectively. (h)–(j) Analogous figures for the segmented piston/tip/tilt mirror. Note: The segmented piston/tip/tilt device does have three actuators per segment.
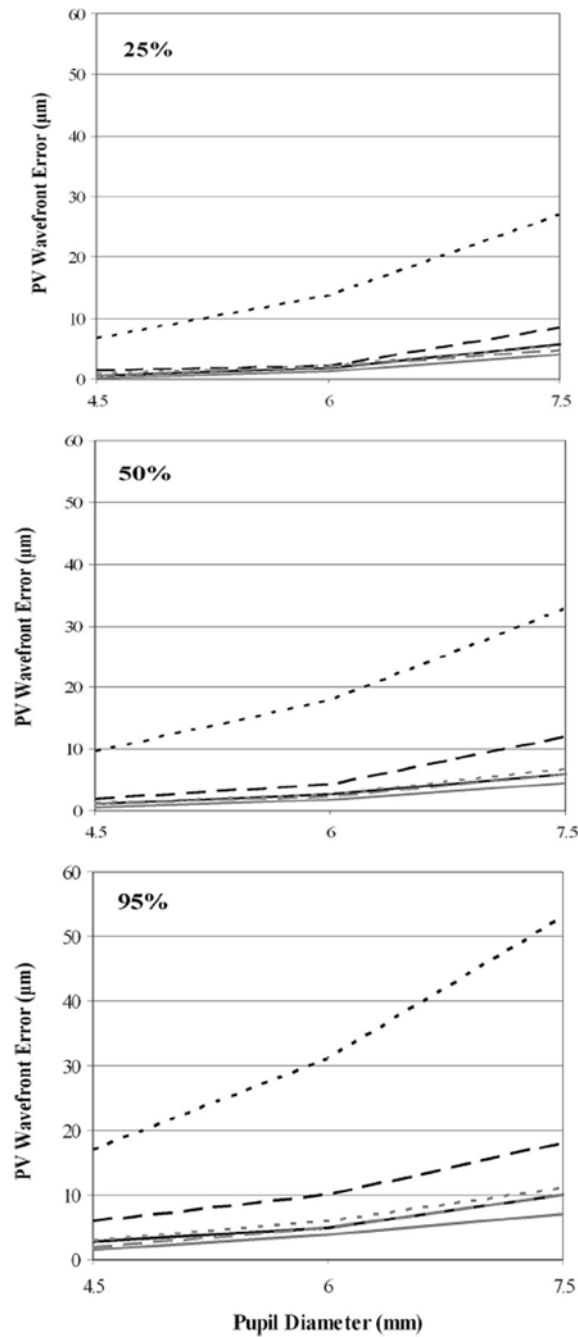
Fig. 4.
PV wavefront error that encompasses 25% (top), 50% (middle), and 95% (bottom) of the
population in the Rochester (black curves) and Indiana (gray curves) populations as a function
of pupil diameter. For the Rochester data, three cases are presented: (i) all aberrations present
(short dashed curves), (ii) all aberrations present with zeroed Zernike defocus (long dashed
curves), and (iii) all aberrations present with zeroed defocus and astigmatism (solid curves).
For the Indiana data, the three cases are (i) residual aberrations after a conventional refraction
using trial lenses (short dashed curves), (ii) all aberrations present with zeroed Zernike defocus
(long dashed curves), and (iii) all aberrations present with zeroed defocus and astigmatism
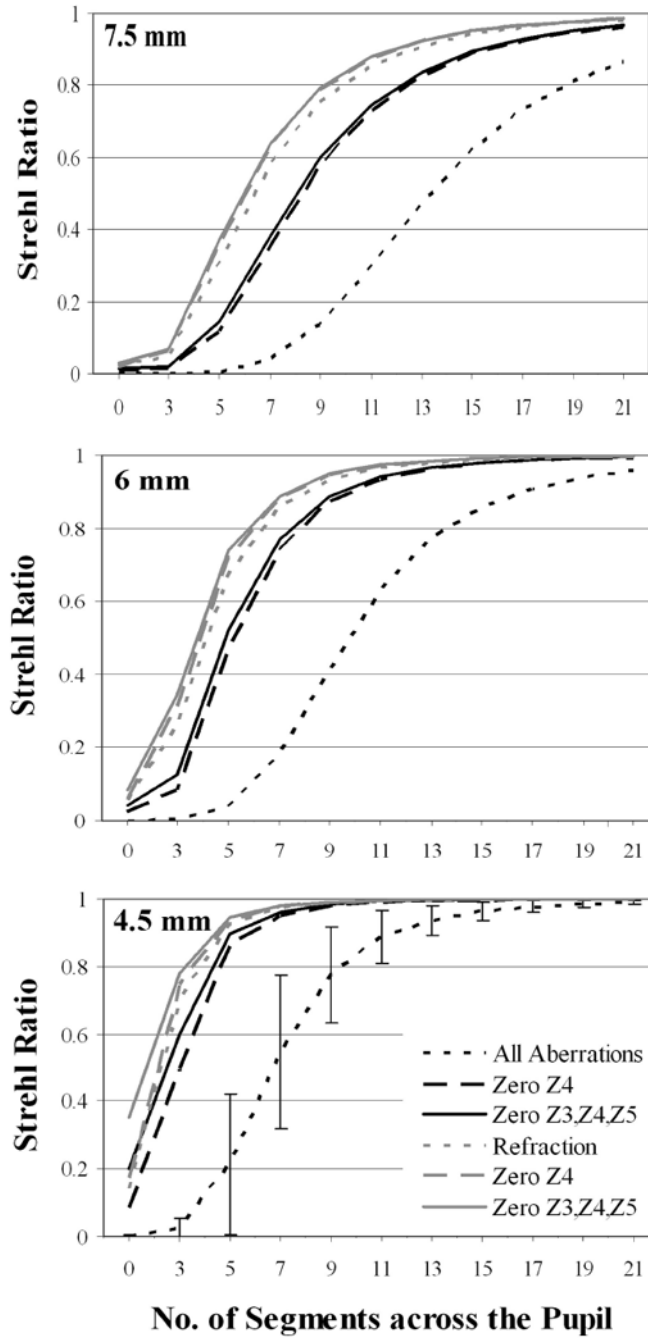(solid curves).
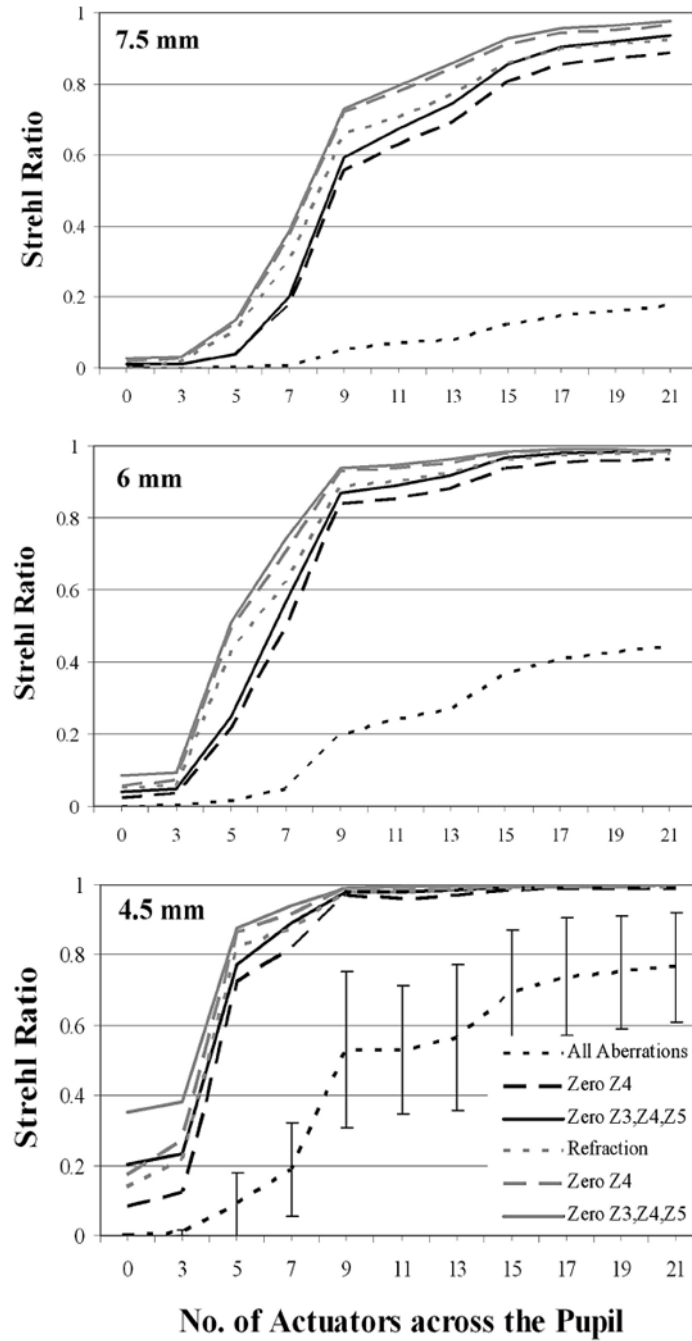
Fig. 5.
Corrected Strehl ratio for discrete actuator DMs as a function of actuator number for pupil diameters of 7.5 (top), 6 (middle), and 4.5 mm (bottom). The wavelength is 0.6 μm. For each plot, three curves are shown for the Rochester (black) and Indiana (gray) populations, and correspond to the presence of all aberrations (short dashed curve), all aberrations with zeroed Zernike defocus (long dashed curves), and all aberrations with zeroed second-order aberrations (solid curves). Note that the all aberrations condition for the Rochester population includes the subject's refractive error, while that for the Indiana population includes only the residual defocus and astigmatism after a sphero-cylindrical correction with trial lenses. The error bars for the single representative curve correspond to ±1 standard deviation.
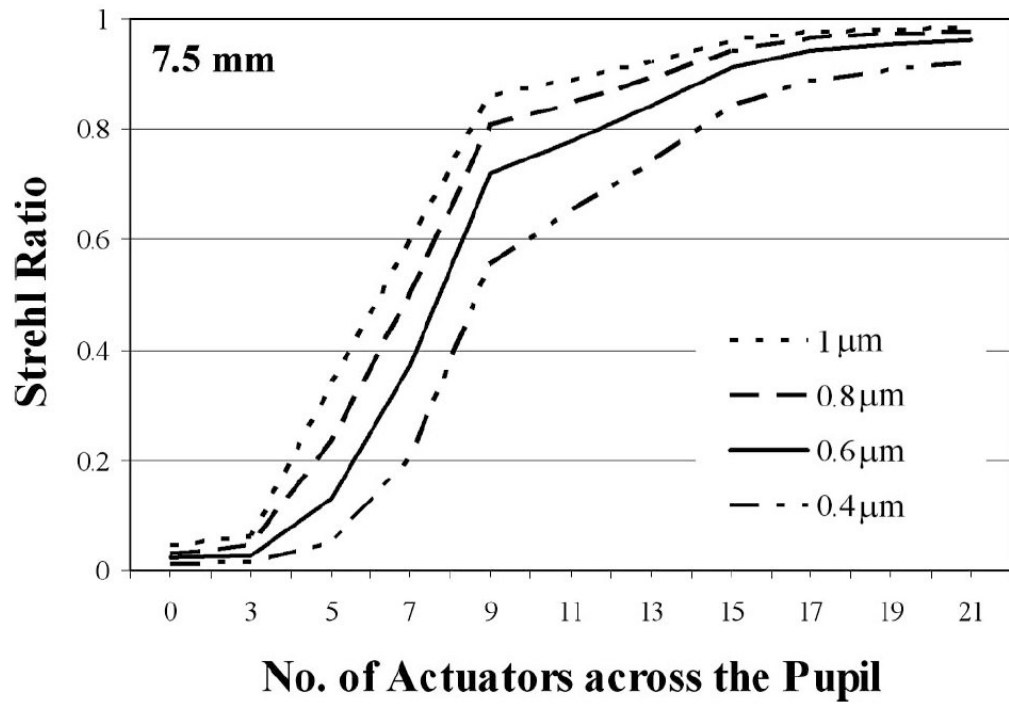
Fig. 6.
Corrected Strehl for different wavelengths (0.4, 0.6, 0.8, and 1 μm) and number of actuators across the 7.5 mm pupil for the Indiana population. Residual defocus was zeroed.
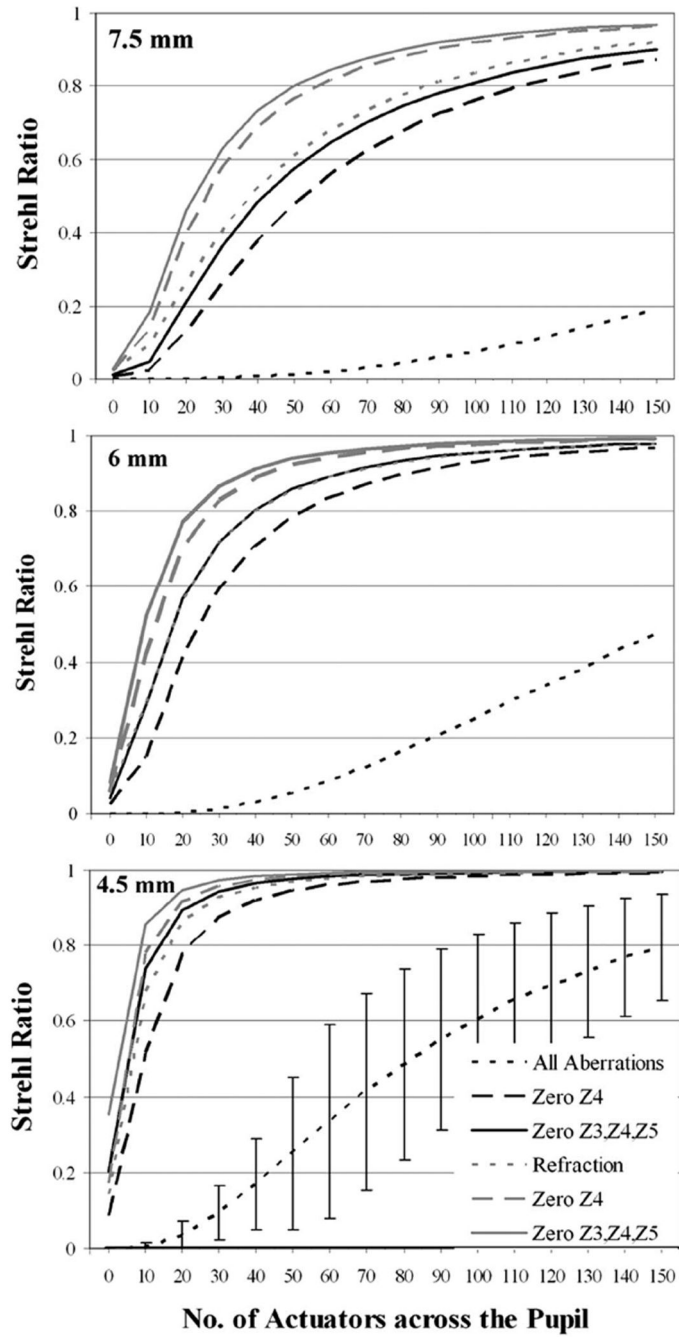
Fig. 7.
Corrected Strehl ratio for piston-only, segmented correctors as a function of segment number for pupil diameters of 7.5 (top), 6 (middle), and 4.5 mm (bottom). The wavelength is 0.6 μm. For each plot, three curves are shown for the Rochester (black) and Indiana (gray) populations and correspond to the presence of all aberrations (short dashed curve), all aberrations with zeroed Zernike defocus (long dashed curves), and all aberrations with zeroed second-order aberrations (solid curves). Note: For the 6 mm pupil diameter, the results for the Indiana population with all aberrations present follows very closely the predicted performance for the Rochester case with zeroed second-order aberrations. The error bars for the single representative curve correspond to ±1 standard deviation.

Fig. 8.
Corrected Strehl ratio for piston/tip/tilt segmented correctors as a function of segment number for pupil diameters of 7.5 (top), 6 (middle), and 4.5 mm (bottom). The wavelength is 0.6 μm. For each plot, three curves are shown for the Rochester (black) and Indiana (gray) populations and correspond to the presence of all aberrations (short dashed curve), all aberrations with zeroed Zernike defocus (long dashed curves), and all aberrations with zeroed second-order aberrations (solid curves). The error bars for the single representative curve correspond to ±1 standard deviation.

Table 1

Predicted Wavefront Corrector Parameters for Diffraction-Limited Imaging in the Eye

Parameter	Value
Temporal bandwidth	1–12 Hz closed loop[a]
Reflectivity	>90% (400–950 nm)
Mirror diameter	4–8 mm
Wavefront requirement (7.5 mm pupil, 95% population)	10–53 µm (Rochester) 7–11 µm (Indiana)
Number of actuators or segments across the pupil diameter (for 0.8 Strehl, 7.5 mm pupil)	>14 (Rochester), 11–14 (Indiana) discrete actuator ≫95 (Rochester), 50–90 (Indiana) piston-only segmented 12–19 (Rochester), 9–10 (Indiana) piston/tip/tilt segmented

[a]References 26 and 27.